

Directional Total Generalized Variation Regularization

Rasmus Dalgas Kongskov* Yiqiu Dong* Kim Knudsen*

September 14, 2022

Abstract

In inverse problems, prior information and priori-based regularization techniques play important roles. In this paper, we focus on image restoration problems, especially on restoring images whose texture mainly follow one direction. In order to incorporate the directional information, we propose a new directional total generalized variation (DTGV) functional, which is based on total generalized variation (TGV) by Bredies *et al.* [SIAM J. Imaging Sci., 3 (2010)]. After studying the mathematical properties of DTGV, we utilize it as regularizer and propose the L^2 -DTGV variational model for solving image restoration problems. Due to the requirement of the directional information in DTGV, we give a direction estimation algorithm, and then apply a primal-dual algorithm to solve the minimization problem. Experimental results show the effectiveness of the proposed method for restoring the directional images. Comparing with isotropic regularizers like total variation and TGV, the improvement of texture preservation and noise removal is significant.

1 Introduction

In the field of inverse problems, regularization techniques have been introduced to overcome the ill-posedness in order to obtain reasonable and stable solutions. For many image processing problems incorporation prior information through regularization techniques has attracted much attention. In this paper, we will study directional regularization on account of the image restoration problems.

Suppose that an image \hat{u} is a real function defined on Ω , a connected bounded open subset of \mathbb{R}^2 with compact Lipschitz boundary, i.e., $\hat{u} : \Omega \rightarrow \mathbb{R}$. The degraded image f is given by

$$f = A\hat{u} + \eta, \quad (1)$$

where $A \in \mathcal{L}(L^2(\Omega))$ is a linear and continuous blurring operator, and η denotes additive white Gaussian noise with mean 0 and variance σ^2 . Based on the Bayes rule and by using a maximum a posteriori (MAP) estimator, we obtain the variational model for restoring \bar{u} as follows:

$$\min_u \frac{1}{2} \|Au - f\|_{L^2(\Omega)}^2 + \lambda \mathcal{R}(u), \quad (2)$$

*Department of Applied Mathematics and Computer Science, Technical University of Denmark, 2800 Kgs. Lyngby, Denmark (rara@dtu.dk, yido@dtu.dk, kiknu@dtu.dk).



Figure 1: Left: A CT scan of uni-directional glass fibre (obtained from [18]). Right: A CT scan and 3D-model of an optical fibre with a cavity (obtained from [25]).

where \mathcal{R} is the regularization term, which is according to the prior information on \hat{u} , and $\lambda > 0$ is the regularization parameter, which controls the trade-off between a good fit of f and the requirements from the regularization.

Due to its capability of preserving sharp edges, total variation (TV) regularization proposed in [24] is very popularly used in many image processing problems, e.g. in image denoising [33, 12, 13, 27], in blind deconvolution [10], in tomographic reconstruction [11, 19], etc. Although TV regularization is very effective for restoring piece-wise constant images, it has some shortcomings, and the most notable one is the appearance of stair-casing artifacts in slanted regions [22, 23]. To overcome stair-casing artifacts, higher-order derivatives have been used, see [26, 9, 28, 30]. In [6], the total generalized variation (TGV) of order h , was proposed. It incorporates smoothness from the first up to the h -th derivative. When h equals 1, it yields the TV regularization.

In many applications, the textures in images have very clear directionality. Here, we call the images whose textures are mainly along one certain direction as *directional images*. For example, fibre materials commonly appears in many real applications, e.g., optical fibres in communication, glass fibres in wind-turbine blades, and ceramic fibres in fuel cells. Imaging techniques are often utilized to visualize then analyze those material properties. In Equation 1, we show a few images related with fibre materials. Achieving high-quality images is crucial for the analysis of these fibre materials, therefore as a very important priori imposing the direction information of the textures in imaging methods is highly desirable.

Directional regularization has been introduced for standard TV in [32, 16] and in terms of shearlet-based TV in [14]. In [2] a type of directional TV is introduced for image denoising based on images with one main direction. This method is further developed to be spatially adaptive in [36] via pixel-specific angle-estimates. Moreover, the directional information through the structure tensor, defined in [34], has been used to extend TV regularization, and the new regularizer is named as the structure tensor total variation (STV), which has been applied in different imaging problems, see [20, 15]. The STV-based methods are inherently dependent on the structure tensor estimation, which therefore determines the performance of the methods. All these directional regularization techniques are introduced in the discrete case, and their mathematical properties are not studied. Furthermore, it is unclear if these TV-based regularizers are able to be extended to incorporate higher-order derivatives, e.g. turned into TGV-based regularizers.

In this paper, we introduce a way of incorporating directionality into currently

existing regularization techniques. We first give the definition of the directional TV (DTV) functional in the continuous case. Further on we generalize it from first order to higher orders, and propose a new higher-order directional functional: the directional TGV (DTGV). Through several equivalent definitions of the DTGV, We show that the incorporating the directional priori into TGV can be boiled down to the modification of the operators, which therefore can be handled easily in numerical implement. Based on the mathematical properties of the DTGV, we apply it as regularization term in Equation 2 for solving image restoration problems, and provide the results of the existence and the uniqueness of a solution to the minimization problem in Equation 2. Since the DTGV requires the input of the main direction of the textures in the image, we also propose a direction estimation algorithm, which can be easily extended to spatially varying direction estimation instead of single one. Then we apply the primal-dual algorithm [8] to solve the minimization problem in Equation 2. The numerical results in this paper show that by using the DTGV as regularizer the degraded directional images are much better restored comparing with the results from the isotropic regularizers, e.g., TV and TGV. The textures in the images are well preserved, and the PSNR values increase more than 2dB.

The rest of the paper is organized as follows. In section 2 we define the directional total variation (DTV) functional. Through two equivalent definitions of the DTV, we obtain a hint of how to incorporate directional information into the TGV. In section 3, we propose the second order directional total generalized variation (DTGV_λ^2) functional, and extend it to higher orders. We study the mathematical properties of the DTGV in section 4, and in section 5 we apply it as regularization in Equation 2 to propose a new L^2 - DTGV_λ^2 model. The existence and uniqueness results for the L^2 - DTGV_λ^2 model is also provided. In section 6 we introduce a direction estimation algorithm in order to obtain the required main direction in corrupted images, and then apply the primal-dual algorithm for solving the minimization problem in our restoration model based on the work proposed in [8]. The numerical results shown in section 7 demonstrate the effectiveness of the direction estimation algorithm, the influence of the parameters in DTGV, and the performance of our restoration method. Finally, conclusions are drawn in section 8.

2 Directional Total Variation

The definition of total variation (TV) for $u \in \text{BV}(\Omega)$, space of functions of bounded variation over domain Ω , can be written as [1, 24]:

$$\text{TV}(u) = \sup \left\{ \int_{\Omega} u \operatorname{div} \mathbf{v} \, dx \mid \mathbf{v} \in C_c^1(\Omega, \mathbb{R}^2), \mathbf{v}(x) \in B_2(0) \, \forall x \in \Omega \right\}, \quad (3)$$

where \mathbf{v} denotes the dual-variable and $B_2(0)$ denotes the Euclidian unit ball centered at the origin. In this section, we will introduce the direction information into TV and define the directional total variational (DTV). The idea of DTV was first proposed in [2] under the discrete case. Following the similar idea, here we will give the DTV definition in the continuous case. Through an example we show the different behavior of TV and DTV. More mathematical properties will be provided based on the extension to total generalized variation (TGV) in Section 3.

TV is rotational invariant. In order to change it into rotational variant, we restrict the dual variable \mathbf{v} in an ellipse instead of the unit ball. Different from an escribed ellipse of the unit ball defined in [2], we introduce an inscribed ellipse such that the maximum axis-length is 1. Clearly the inscribed ellipse is bounded by the unit ball, and this boundedness will be utilized when we study the mathematical properties in Section 3. We give the definition of the inscribed ellipse as follows.

Definition 2.1. We define the elliptical set, $E^{a,\theta}(0)$, centered at the origin with the major semi-axis 1 and the minor semi-axis a and $a \in (0, 1]$ as

$$E^{a,\theta}(0) = \left\{ \begin{pmatrix} x_1 \\ x_2 \end{pmatrix} \in \mathbb{R}^2 \left| \left(\frac{x_1 \cos \theta + x_2 \sin \theta}{1} \right)^2 + \left(\frac{-x_1 \sin \theta + x_2 \cos \theta}{a} \right)^2 \leq 1 \right. \right\},$$

where the angle $\theta \in]-\pi, \pi]$ measures the rotation with respect to the Cartesian coordinate system $x = (x_1, x_2)^\top$ counter-clockwisely from the x_1 -axis to the major semi-axis.

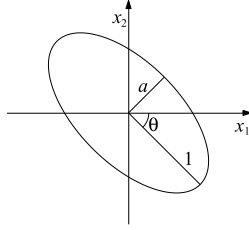


Figure 2: Sketch of ellipse $E^{a,\theta}(0)$. Here shown for $a = 0.5$ and $\theta = -\frac{\pi}{4}$.

We have sketched $E^{a,\theta}(0)$ in Figure 2. Based on the definition of the elliptical set, we now are ready to define DTV in the continuous case.

Definition 2.2. With the definition of $E^{a,\theta}(0)$ in 2.1, the directional total variation (DTV) of a function $u \in \text{BV}(\Omega)$ is defined as

$$\text{DTV}(u) = \sup \left\{ \int_{\Omega} u \operatorname{div} \tilde{\mathbf{v}} \, dx \mid \tilde{\mathbf{v}} \in C_c^1(\Omega, \mathbb{R}^2), \tilde{\mathbf{v}}(x) \in E^{a,\theta}(0) \, \forall x \in \Omega \right\}.$$

Based on the invertible transformation between the points in $B_2(0)$ and $E^{a,\theta}(0)$, we have

$$\tilde{\mathbf{v}}(x) = R_{\theta} \Lambda_a \mathbf{v}(x) \quad \text{and} \quad \mathbf{v}(x) = \Lambda_{\frac{1}{a}} R_{-\theta} \tilde{\mathbf{v}}(x) \quad \text{for } \forall x \in \Omega, \quad (4)$$

where $\mathbf{v}(x)$ and $\tilde{\mathbf{v}}(x)$ are in $B_2(0)$ and $E^{a,\theta}(0)$ respectively, R_{θ} is a rotation matrix, Λ_a is a scaling matrices, and they defined as

$$R_{\theta} = \begin{pmatrix} \cos \theta & -\sin \theta \\ \sin \theta & \cos \theta \end{pmatrix} \quad \text{and} \quad \Lambda_a = \begin{pmatrix} 1 & 0 \\ 0 & a \end{pmatrix}.$$

According to the relations in Equation 4, we give another equivalent definition for DTV.

Definition 2.3. For a function $u \in \text{BV}(\Omega)$, its DTV is defined as

$$\text{DTV}(u) = \sup \left\{ \int_{\Omega} u \operatorname{div} R_{\theta} \Lambda_a \mathbf{v} \, dx \mid \mathbf{v} \in C_c^1(\Omega, \mathbb{R}^2), \mathbf{v}(x) \in B_2(0) \, \forall x \in \Omega \right\}.$$

This definition is very similar as the one for TV in Equation 3, and the only difference is the rotation and scaling matrices in the integral. Here, we provide an example to show the difference between DTV and TV.

Example 2.4. Define $u = \mathcal{X}_{rB_2(0)}$, which is an indicator function of a disk in \mathbb{R}^2 centered at the origin with radius r , i.e., $u(x) = 1$ if $\|x\|_2 \leq r$; otherwise $u(x) = 0$. Based on the definition in (3), we can easily obtain $\text{TV}(u) = 2\pi r$. The calculation of $\text{DTV}(u)$ is according to 2.3. By using the divergence theorem, we have

$$\begin{aligned} \int_{\Omega} u \operatorname{div} R_{\theta} \Lambda_a \mathbf{v} \, dx &= \int_{\mathcal{X}_{rB_2(0)}} \operatorname{div} R_{\theta} \Lambda_a \mathbf{v} \, dx \\ &= \int_{\partial \mathcal{X}_{rB_2(0)}} (R_{\theta} \Lambda_a \mathbf{v}) \cdot \mathbf{n} \, dx. \end{aligned}$$

Because of $\mathbf{v}(x) \in B_2(0)$, for simplicity we change into the polar coordinates with $\kappa \in [0, 1]$ and $\phi \in [0, 2\pi]$ and obtain

$$\begin{aligned} \int_{\Omega} u \operatorname{div} R_{\theta} \Lambda_a \mathbf{v} \, dx &= r \int_0^{2\pi} \left(R_{\theta} \Lambda_a \begin{pmatrix} \kappa \cos(\tau + \phi) \\ \kappa \sin(\tau + \phi) \end{pmatrix} \right) \cdot \begin{pmatrix} \cos(\tau) \\ \sin(\tau) \end{pmatrix} \, d\tau \\ &= r\kappa \int_0^{2\pi} [(\cos(\theta) \cos(\tau + \phi) - a \sin(\theta) \sin(\tau + \phi)) \cos(\tau) \\ &\quad + (\sin(\theta) \cos(\tau + \phi) + a \cos(\theta) \sin(\tau + \phi)) \sin(\tau)] \, d\tau \\ &= r\pi(a + 1)\kappa \cos(\theta + \phi). \end{aligned}$$

Then,

$$\text{DTV}(u) = \sup_{\substack{\kappa \in [0, 1] \\ \phi \in [0, 2\pi]}} r\pi(a + 1)\kappa \cos(\theta + \phi) = r\pi(a + 1).$$

Clearly, when $a = 1$ we have $\text{TV}(u) = \text{DTV}(u)$. In this case, DTV is same as TV. Otherwise, we have $\text{DTV}(u) < \text{TV}(u)$, since $a \in (0, 1]$.

In imaging problems a common artifact by using TV as regularization is the staircasing effect, which is a classical example of a mismatch between prior knowledge and the reality, i.e., smooth regions are approximated by piecewise constant regions during image reconstruction. One way to overcome the staircasing effect is to use higher order derivatives in the regularization. One successful work along this way is total generalized variation (TGV) [6]. In the next section, we will follow the similar idea as from TV to DTV to incorporate direction information into TGV.

3 Directional Total Generalized Variation

Total Generalized Variation (TGV) is a generalization of TV to a functional which takes derivatives of order $h > 0$ into account, and the first order TGV,

i.e., $h = 1$, is identical to TV. In practical applications, such as various image processing problems, the second order TGV is often used, since a piecewise affine prior fits natural images better than a piecewise constant prior. It turns out that regularizing a denoising problem with the second order TGV yields improved results compared to TV and the staircasing effect is well avoided [6]. The second order TGV of a function u is defined as:

$$\begin{aligned} \text{TGV}_\lambda^2(u) = \sup \left\{ \int_\Omega u \operatorname{div}^2 W \, dx \right\} \\ W \in C_c^2(\Omega, \operatorname{Sym}^2(\mathbb{R}^2)), \|W(x)\|_F \leq \lambda_0, \|(\operatorname{div} W(x))^\top\|_2 \leq \lambda_1 \, \forall x \in \Omega \}, \end{aligned} \quad (5)$$

where $\lambda_0, \lambda_1 \in \mathbb{R}_+$ denote positive weights, and $\operatorname{Sym}^2(\mathbb{R}^2)$ is the space of 2-by-2 symmetric matrices. We set a 2-by-2 symmetric matrix $V = \begin{pmatrix} v_{11} & v_{12} \\ v_{12} & v_{22} \end{pmatrix}$, and define

$$(\operatorname{div} V)^\top = \begin{pmatrix} \frac{\partial v_{11}}{\partial x_1} + \frac{\partial v_{12}}{\partial x_2} \\ \frac{\partial v_{21}}{\partial x_1} + \frac{\partial v_{22}}{\partial x_2} \end{pmatrix} \in \mathbb{R}^2, \quad \operatorname{div}^2 V = \frac{\partial^2 v_{11}}{\partial x_1^2} + \frac{\partial^2 v_{22}}{\partial x_2^2} + 2 \frac{\partial^2 v_{12}}{\partial x_1 \partial x_2}.$$

In order to incorporate direction information into TGV_λ^2 , based on the equivalence between Frobenius norm and 2-norm, we give another definition of TGV_λ^2

$$\begin{aligned} \text{TGV}_\lambda^2(u) = \sup \left\{ \int_\Omega u \operatorname{div}^2 W \, dx \right\} \\ W \in C_c^2(\Omega, \operatorname{Sym}^2(\mathbb{R}^2)), W(x) \in \lambda_0 B_{2 \times 2}(0), (\operatorname{div} W(x))^\top \in \lambda_1 B_2(0) \, \forall x \in \Omega \}, \end{aligned} \quad (6)$$

where $B_{2 \times 2}(0)$ denotes the unit high order sphere, i.e., if $V = \begin{pmatrix} v_{11} & v_{12} \\ v_{21} & v_{22} \end{pmatrix} \in B_{2 \times 2}(0)$ then $(v_{i1}, v_{i2})^\top \in B_2(0)$ and $(v_{1i}, v_{2i})^\top \in B_2(0)$ with $i = 1, 2$. Then, $W(x) \in \lambda_0 B_{2 \times 2}(0)$ means $\|W(x)\|_2 \leq \lambda_0$.

Following similar idea as from TV to DTV, in order to modify TGV_λ^2 to rotational variant, we replace the ball and the high order sphere by elliptical sets, and define a new functional: directional total generalized variation (DTGV).

Definition 3.1. The second order directional total generalized variation, DTGV_λ^2 , of a function $u \in L^1(\Omega)$ is defined as

$$\begin{aligned} \text{DTGV}_\lambda^2(u) = \sup \left\{ \int_\Omega u \operatorname{div}^2 \widetilde{W} \, dx \right\} \\ \widetilde{W} \in C_c^2(\Omega, \operatorname{Sym}^2(\mathbb{R}^2)), \widetilde{W}(x) \in \lambda_0 E_{2 \times 2}^{a, \theta}(0), (\operatorname{div} \widetilde{W}(x))^\top \in \lambda_1 E_2^{a, \theta}(0) \, \forall x \in \Omega \}, \end{aligned} \quad (7)$$

where $E_{2 \times 2}^{a, \theta}(0)$ denotes a high order elliptical set. If $V = \begin{pmatrix} v_{11} & v_{12} \\ v_{21} & v_{22} \end{pmatrix} \in E_{2 \times 2}^{a, \theta}(0)$, then we have $(v_{i1}, v_{i2})^\top \in E^{a, \theta}(0)$ and $(v_{1i}, v_{2i})^\top \in E^{a, \theta}(0)$ with $i = 1, 2$.

Next, we will provide another equivalent definition for DTGV_λ^2 , which has the same feasible set as in (5). We will show that comparing with the definition of TGV_λ^2 in (5), the only difference is on the operators div^2 and div .

To derive this result, we need the invertible transformation between $B_{2 \times 2}(0)$ and $E_{2 \times 2}^{a, \theta}(0)$, which can be easily obtained based on their definitions. Let $V \in B_{2 \times 2}(0)$ and $\widetilde{V} \in E_{2 \times 2}^{a, \theta}(0)$, then we have

$$\widetilde{V} = R_\theta \Lambda_a V \Lambda_a R_{-\theta}, \quad (8)$$

where R_θ and Λ_a are the rotation matrix and scaling matrix, respectively, which have been defined in [section 2](#). In addition, we define the directional divergence, $\widetilde{\text{div}}$, as

$$\widetilde{\text{div}} = \text{div} R_\theta \Lambda_a, \quad (9)$$

and the second order directional divergence, $\widetilde{\text{div}}^2$, as

$$\widetilde{\text{div}}^2 = \Lambda_a R_{-\theta} H R_\theta \Lambda_a \quad \text{with} \quad H = \begin{pmatrix} \partial_{x_1 x_1} & \partial_{x_1 x_2} \\ \partial_{x_1 x_2} & \partial_{x_2 x_2} \end{pmatrix}. \quad (10)$$

Now we are ready to prove the following equivalent definition for DTGV_λ^2 , which is much more convenient for the derivation of the numerical algorithms.

Theorem 3.2. *With the directional divergence and the second order directional divergence defined in [Equation 9](#) and [Equation 10](#), the second order directional total generalized variation (DTGV_λ^2) of a function $u \in L^1(\Omega)$ can be reformulated as:*

$$\text{DTGV}_\lambda^2(u) = \sup \left\{ \int_\Omega u \widetilde{\text{div}}^2 W \, dx \mid \begin{aligned} & W \in C_c^2(\Omega, \text{Sym}^2(\mathbb{R}^2)), \|W(x)\|_2 \leq \lambda_0, \|(\widetilde{\text{div}} W(x))^\top\|_2 \leq \lambda_1 \, \forall x \in \Omega \end{aligned} \right\}. \quad (11)$$

Proof: Let \widetilde{W} be a function in the feasible set of the supremum problem in [Equation 7](#), i.e., $\widetilde{W} \in C_c^2(\Omega, \text{Sym}^2(\mathbb{R}^2))$ with $\widetilde{W}(x) \in \lambda_0 E_{2 \times 2}^{a, \theta}(0)$ and $(\text{div} \widetilde{W}(x))^\top \in \lambda_1 E_2^{a, \theta}(0)$ for any $x \in \Omega$.

Based on the invertible transformation in [Equation 8](#), we get

$$W(x) = \Lambda_{\frac{1}{a}} R_{-\theta} \widetilde{W}(x) R_\theta \Lambda_{\frac{1}{a}},$$

and have $W(x) \in \lambda_0 B_{2 \times 2}(0)$, i.e., $\|W(x)\|_2 \leq \lambda_0$, for any $x \in \Omega$. In addition, because of $(\text{div} \widetilde{W}(x))^\top \in \lambda_1 E_2^{a, \theta}(0)$, according to the invertible transformation between unit ball and elliptical set given in [Equation 4](#), we obtain

$$\Lambda_{\frac{1}{a}} R_{-\theta} (\text{div} \widetilde{W}(x))^\top = \Lambda_{\frac{1}{a}} R_{-\theta} (\text{div} R_\theta \Lambda_a W(x) \Lambda_a R_{-\theta})^\top = (\widetilde{\text{div}} W(x))^\top \in \lambda_1 B_2(0),$$

i.e., $\|(\widetilde{\text{div}} W(x))^\top\|_2 \leq \lambda_1$. Hence, we have proved that the feasible set in [Equation 11](#) is equivalent to the one in [Equation 7](#).

Moreover, by using the transformation in [Equation 8](#) and the definition of $\widetilde{\text{div}}^2$ in [Equation 10](#), we have

$$\begin{aligned} \text{div}^2 \widetilde{W}(x) &= H : \widetilde{W}(x) \\ &= H : (R_\theta \Lambda_a W(x) \Lambda_a R_{-\theta}) \\ &= (\Lambda_a R_{-\theta} H R_\theta \Lambda_a) : W(x) \\ &= \widetilde{\text{div}}^2 W(x), \end{aligned}$$

where “:” denotes the Frobenius inner product, i.e., $H : \widetilde{W}(x) = \partial_{x_1 x_1} w_{11} + 2\partial_{x_1 x_2} w_{12} + \partial_{x_2 x_2} w_{22}$ with $\widetilde{W}(x) = \begin{pmatrix} w_{11} & w_{12} \\ w_{12} & w_{22} \end{pmatrix}$, and the third equality is obtained by straightforward calculation.

Therefore, the definition of DTGV_λ^2 in Equation 11 is equivalent to the one in Equation 7. \square

In this end of this section, we will extend the definition of DTGV_λ^2 in Equation 11 to arbitrary order $h \in \mathbb{N}$. In [6], TGV_λ^h has been defined for any $h \in \mathbb{N}$:

$$\begin{aligned} \text{TGV}_\lambda^h(u) &= \sup \left\{ \int_\Omega u \operatorname{div}^h \mathbf{w} \, dx \right\} \\ \mathbf{w} &\in C_c^h(\Omega, \operatorname{Sym}^h(\mathbb{R}^2)), \|\operatorname{div}^l \mathbf{w}(x)\|_2 \leq \lambda_l, \forall x \in \Omega \text{ and } l = 0, \dots, h-1 \end{aligned} \quad (12)$$

where $\operatorname{Sym}^h(\mathbb{R}^2)$ denotes the space of symmetric h -tensors in \mathbb{R}^2 . For any $x \in \Omega$, $\mathbf{w}(x)$ is an h -tensor. The operator div^l on $\mathbf{w}(x)$ is defined as

$$(\operatorname{div}^l \mathbf{w}(x))_b = \sum_{\gamma \in N_l} \frac{l!}{\gamma!} \frac{\partial^l \mathbf{w}(x)_{b+\gamma}}{\partial x^\gamma} \quad \text{for each component } b \in N_{h-l}$$

where $N_h = \left\{ b \in \mathbb{N}^2 \mid |b| = \sum_{i=1}^2 b_i = h \right\}$. In addition, $\|\cdots\|_2$ on a symmetric h -tensor is defined as

$$\|\mathbf{w}(x)\|_2 = \left(\sum_{b \in N_h} \frac{h!}{b!} \mathbf{w}_b(x)^2 \right)^{1/2}.$$

For further details of the h -tensors we refer the reader to [6].

To take the direction information into account, referring to the results in Equation 11 we need define l -directional divergence, $\widetilde{\operatorname{div}}^l$ with $l \in \mathbb{N}$. With the directional divergence $\widetilde{\operatorname{div}}$ defined in Equation 9 we can obtain $\widetilde{\operatorname{div}}^l$ for any order l based on $\widetilde{\operatorname{div}}^{k+l} \mathbf{w}(x) = \widetilde{\operatorname{div}}^k \widetilde{\operatorname{div}}^l \mathbf{w}(x)$. Then, we give the definition of DTGV_λ^h as follows.

Definition 3.3. The h 'th-order directional total generalized variation, DTGV_λ^h , of a function $u \in L^1(\Omega)$ is defined as

$$\begin{aligned} \text{DTGV}_\lambda^h(u) &= \sup \left\{ \int_\Omega u \widetilde{\operatorname{div}}^h \mathbf{w} \, dx \right\} \\ \mathbf{w} &\in C_c^h(\Omega, \operatorname{Sym}^h(\mathbb{R}^2)), \|\widetilde{\operatorname{div}}^l \mathbf{w}(x)\|_2 \leq \lambda_l, \forall x \in \Omega \text{ and } l = 0, \dots, h-1 \end{aligned} \quad (13)$$

Following the similar idea as the proof of 3.2, we will obtain another equivalent definition for DTGV_λ^h .

Definition 3.4. For a function $u \in L^1(\Omega)$, $\text{DTGV}_\lambda^h(u)$ can be reformulated as

$$\begin{aligned} \text{DTGV}_\lambda^h(u) &= \sup \left\{ \int_\Omega u \operatorname{div}^h \mathbf{w} \, dx \right\} \\ \mathbf{w} &\in C_c^h(\Omega, \operatorname{Sym}^h(\mathbb{R}^2)), \operatorname{div}^l \mathbf{w}(x) \in \lambda_l \underbrace{E_{2 \times \dots \times 2}^{a, \theta}}_{h-l \text{ times}}(0), \forall x \in \Omega \text{ and } l = 0, \dots, h-1 \end{aligned} \quad (14)$$

Clearly, for $h = 1$ and $\lambda = 1$, we have $\text{DTGV}_1^1(u) = \text{DTV}(u)$.

4 Properties of DTGV

In this section, we will derive some properties of DTGV_λ^h on the space of *Bounded Generalized Variation* of order h (BGV^h), which is defined as

$$\text{BGV}^h(\Omega) = \left\{ u \in L^1(\Omega) \mid \text{TGV}_\lambda^h(u) < \infty \right\}.$$

When $\text{BGV}^h(\Omega)$ is equipped with the norm

$$\|u\|_{\text{BGV}^h} = \|u\|_1 + \text{TGV}_\lambda^h(u),$$

it is a Banach space [6]. In the following two propositions, we will show that DTGV_λ^h is an equivalent semi-norm as TGV_λ^h on $\text{BGV}^h(\Omega)$.

Proposition 1. $\text{DTGV}_\lambda^h : \text{BGV}^h(\Omega) \rightarrow \mathbb{R}$ is a semi-norm.

Proof: Based on the definition of DTGV_λ^h , it is obvious that $\text{DTGV}_\lambda^h(u) \geq 0$. Further, with the linearity of the integral we have

$$\text{DTGV}_\lambda^h(tu) = |t| \text{DTGV}_\lambda^h(u).$$

Define the feasible set of the supremum problem in Equation 13 as:

$$K_D = \left\{ \mathbf{w} \in C_c^h(\Omega, \text{Sym}^h(\mathbb{R}^2)) \mid \|\widetilde{\text{div}}^l \mathbf{w}(x)\|_2 \leq \lambda_l, \forall x \in \Omega \text{ and } l = 0, \dots, h-1 \right\}.$$

Then, we have that for $u_1, u_2 \in \text{BGV}_\lambda^h$

$$\begin{aligned} \text{DTGV}_\lambda^h(u_1 + u_2) &= \sup_{\mathbf{w} \in K_D} \int_{\Omega} (u_1 + u_2) \widetilde{\text{div}}^h \mathbf{w} \, dx \\ &\leq \sup_{\mathbf{w} \in K_D} \int_{\Omega} u_1 \widetilde{\text{div}}^h \mathbf{w} \, dx + \sup_{\mathbf{w} \in K_D} \int_{\Omega} u_2 \widetilde{\text{div}}^h \mathbf{w} \, dx \\ &= \text{DTGV}_\lambda^h(u_1) + \text{DTGV}_\lambda^h(u_2). \end{aligned}$$

In addition, according to the definition of DTGV_λ^h we clearly have $\text{DTGV}_\lambda^h(u) = 0$ with any constant function u . Therefore, we conclude that DTGV_λ^h is a semi-norm on $\text{BGV}^h(\Omega)$. \square

Proposition 2. For a function $u \in L^1(\Omega)$, we have

$$a^h \frac{\min_{l \in \{0, h-1\}} \lambda_l}{\max_{l \in \{0, h-1\}} \lambda_l} \text{TGV}_\lambda^h(u) \leq \text{DTGV}_\lambda^h(u) \leq \text{TGV}_\lambda^h(u). \quad (15)$$

Proof: Define the feasible sets of the supremum problems in the definitions of DTGV in Equation 14 and TGV in Equation 12 respectively as

$$\begin{aligned} K_E &= \left\{ \mathbf{w} \in C_c^h(\Omega, \text{Sym}^h(\mathbb{R}^2)) \mid \text{div}^l \mathbf{w} \in \lambda_l \underbrace{E_2^{\alpha, \theta} \times \dots \times 2}_{h-l \text{ times}}(0), l = 0, \dots, h-1 \right\}. \\ K_B &= \left\{ \mathbf{w} \in C_c^h(\Omega, \text{Sym}^h(\mathbb{R}^2)) \mid \text{div}^l \mathbf{w} \in \lambda_l \underbrace{B_2 \times \dots \times 2}_{h-l \text{ times}}(0), l = 0, \dots, h-1 \right\}. \end{aligned}$$

Since $E_{2 \times \dots \times 2}^{a, \theta}(0)$ is inscribed in $B_{2 \times \dots \times 2}(0)$, then we have $K_E \subset K_B$. Further, due to the same objective function, we can easily get $\text{DTGV}_\lambda^h(u) \leq \text{TGV}_\lambda^h(u)$.

If we shrink the set K_B to

$$K_{\tilde{B}} = \left\{ \mathbf{w} \in C_c^h(\Omega, \text{Sym}^h(\mathbb{R}^2)) \mid \text{div}^l \mathbf{w} \in a^h \lambda_l \underbrace{B_{2 \times \dots \times 2}(0)}_{h-l \text{ times}}, l = 0, \dots, h-1 \right\},$$

then we have $K_{\tilde{B}} \subset K_E$. Further, we obtain the inequality

$$\sup_{\mathbf{w} \in K_{\tilde{B}}} \int_{\Omega} u \text{div}^h \mathbf{w} \, dx \leq \sup_{\mathbf{w} \in K_E} \int_{\Omega} u \text{div}^h \mathbf{w} \, dx,$$

that is, $\text{TGV}_{a^h \lambda}^h(u) \leq \text{DTGV}_\lambda^h(u)$. Based on the third statement in proposition 3.3 in [6], we have the relation between TGV-functionals with different weights as:

$$c \text{TGV}_\lambda^h(u) \leq \text{TGV}_{a^h \lambda}^h(u) \quad \text{with} \quad c = a^h \frac{\min_{l \in \{0, h-1\}} \lambda_l}{\max_{l \in \{0, h-1\}} \lambda_l}.$$

Hence, $c \text{TGV}_\lambda^h(u) \leq \text{DTGV}_\lambda^h(u)$. \square

There are two straightforward results from 2. One is that the semi-norms TGV_λ^h and DTGV_λ^h are equivalent, then we can state an alternative definition of the Banach space $\text{BGV}^h(\Omega)$

$$\text{BGV}^h(\Omega) = \left\{ u \in L^1(\Omega) \mid \text{DTGV}_\lambda^h(u) < \infty \right\} \quad \text{with} \quad \|u\|_{\text{BGV}_\lambda^h} = \|u\|_1 + \text{DTGV}_\lambda^h(u).$$

Another one is that the functional DTGV_λ^h shares the same null space as TGV_λ^h . According to the second statement in proposition 3.3 in [6], we give the following corollary.

Corollary 1. $\text{DTGV}_\lambda^h(u) = 0$ if and only if u is a polynomial of degree less than h .

Since we will utilize DTGV as regularization to build a minimization problem, whose minimizer is our expected estimation to the true image, in the next proposition we will give another property of DTGV, which will be used for proving the existence and uniqueness of a solution to the minimization problem.

Proposition 3. $\text{DTGV}_\lambda^h : \text{BGV}^h \rightarrow \mathbb{R}^+ \cup \{0\}$ is convex and lower semi-continuous.

Proof: For $u_1, u_2 \in L^1(\Omega)$ and $t \in [0, 1]$ we have

$$\begin{aligned} \text{DTGV}_\lambda^h(tu_1 + (1-t)u_2) &= \sup_{\mathbf{w} \in K_E} \int_{\Omega} (tu_1 + (1-t)u_2) \widetilde{\text{div}}^h \mathbf{w} \, dx \\ &\leq t \sup_{\mathbf{w} \in K_E} \int_{\Omega} u_1 \widetilde{\text{div}}^h \mathbf{w} \, dx + (1-t) \sup_{\mathbf{w} \in K_E} \int_{\Omega} u_2 \widetilde{\text{div}}^h \mathbf{w} \, dx \\ &= t \text{DTGV}_\lambda^h(u_1) + (1-t) \text{DTGV}_\lambda^h(u_2). \end{aligned}$$

Hence, DTGV_λ^h is convex.

By use of Fatou's lemma we can show the lower semi-continuity of DTGV_λ^h . Let $\{u_n\}_{n \in \mathbb{N}}$ be a Cauchy sequence in $\text{BGV}^h(\Omega)$ such that $u_n \rightarrow u$ in $L^1(\Omega)$.

Based on the definition of DTGV_λ^h in Equation 14 and Fatou's Lemma, for any $\mathbf{w} \in K_E$ we have

$$\liminf_{n \rightarrow \infty} \text{DTGV}_\lambda^h(u_n) \geq \liminf_{n \rightarrow \infty} \int_{\Omega} u_n \operatorname{div}^h \mathbf{w} \, dx \geq \int_{\Omega} \liminf_{n \rightarrow \infty} u_n \operatorname{div}^h \mathbf{w} \, dx = \int_{\Omega} u \operatorname{div}^h \mathbf{w} \, dx.$$

Taking the supremum over all \mathbf{w} in K_E thus yields

$$\text{DTGV}_\lambda^h(u) \leq \liminf_{n \rightarrow \infty} \text{DTGV}_\lambda^h(u_n),$$

which means that DTGV_λ^h is indeed lower semi-continuous. \square

In the end of the section, we give another equivalent definition for DTGV_λ^2 , which is much easier to use for computational reason.

Theorem 4.1. *For $\Omega \subset \mathbb{R}^2$ and $u \in L^1(\Omega)$ we have*

$$\text{DTGV}_\lambda^2(u) = \min_{v \in \text{BD}(\Omega)} \lambda_1 \|\tilde{D}u - v\|_{\mathcal{M}} + \lambda_0 \|\tilde{\mathcal{E}}v\|_{\mathcal{M}},$$

where $\text{BD}(\Omega)$ denotes the space of vector fields of Bounded Deformation [31], $\|\tilde{D}u\|_{\mathcal{M}} = \int_{\Omega} d|\tilde{D}u| = \text{DTV}(u)$, the directional symmetrized derivative $\tilde{\mathcal{E}}$ is the adjoint operator of $\tilde{\operatorname{div}}$ for a vector field.

Since the proof of 4.1 is following the same lines as the proof of Theorem 3.1 in [7] except the change on the divergence operator, for more details we refer the readers to this paper. In addition, in Section subsection 6.1 we give definitions of all operators under the discrete case.

5 L^2 - DTGV_λ^2 Model

After the study on the properties of DTGV , we are ready to use it as regularization in order to obtain a stable solution of the inverse problem defined in (1). Taking the computational complexity into account, we only apply the second order DTGV , i.e., DTGV_λ^2 . Due to the additive white Gaussian noise model, by combining with the L^2 -data-fidelity term we give our image restoration model as

$$\min_{u \in \text{BGV}^2(\Omega)} \mathcal{J}(u) := \frac{1}{2} \|Au - f\|_{L^2(\Omega)}^2 + \text{DTGV}_\lambda^2(u), \quad (16)$$

which we name as the L^2 - DTGV_λ^2 model. Based on the properties of DTGV_λ^2 and $\text{BGV}^2(\Omega)$, we prove the existence and uniqueness of a solution to (16).

Theorem 5.1. *Suppose that f is in $L^2(\Omega)$ and $A \in \mathcal{L}(L^2(\Omega))$ is a linear and continuous blurring operator, which is injective on the space of affine functions $\mathcal{A}^1(\Omega)$. Then, the L^2 - DTGV_λ^2 model defined in Equation 16 admits a solution. Moreover, if A does not annihilate constant functions, i.e., $A1 \neq 0$, then the solution is unique.*

Proof: Since \mathcal{J} is bounded below, we can choose a minimizing sequence $\{u_n\}_{n \in \mathbb{N}} \subset \text{BGV}^2(\Omega)$ for Equation 16. So both $\{\|Au_n - f\|_2\}$ and $\{\text{DTGV}_\lambda^2(u_n)\}$ with $n = 1, 2, \dots$ are bounded.

Let $P : L^2(\Omega) \rightarrow \mathcal{A}^1(\Omega)$ be a linear projection onto the space of affine functions $\mathcal{A}^1(\Omega)$. Based on the result in proposition 4.1 in [7], we can find a constant $C > 0$ such that

$$\|u\|_2 \leq C \text{TGV}_\lambda^2(u)$$

for any u in $\ker P$, which is a subset of $L^2(\Omega)$. Recall the result in Equation 15, then we have

$$\|u\|_2 \leq \tilde{C} \text{DTGV}_\lambda^2(u) \quad \forall u \in \ker P \subset L^2(\Omega),$$

with $\tilde{C} = \frac{C \max\{\lambda_0, \lambda_1\}}{a^2 \min\{\lambda_0, \lambda_1\}}$. Thank to $\text{DTGV}_\lambda^2(Pu) = 0$ according to 1, by using the triangle inequality on the semi-norm DTGV_λ^2 we obtain $\text{DTGV}_\lambda^2(u) = \text{DTGV}_\lambda^2(u - Pu)$. Hence, we have that $\{u_n - Pu_n\}_{n \in \mathbb{N}}$ is bounded in $L^2(\Omega)$.

Since A is injective on the finite-dimensional space $\mathcal{A}^1(\Omega)$, there is a $C_1 > 0$ such that $\|Pu\|_2 \leq C_1 \|APu\|_2$. Further,

$$\begin{aligned} \|Pu_n\|_2 &\leq C_1 \|APu_n\|_2 \\ &\leq C_1 (\|Au_n - f\|_2 + \|A(u_n - Pu_n) - f\|_2) \leq C_2, \end{aligned}$$

for some $C_2 > 0$. It implies that $\{u_n\}$ is bounded in $L^2(\Omega)$.

Therefore, there exists a weakly convergent subsequence with limit $u^* \in L^2(\Omega)$. Based on the lower semi-continuity of DTGV_λ^2 stated in 3 and Fatou's lemma, we obtain that u^* is a solution of the model Equation 16.

Based on 3, the model Equation 16 is convex. Furthermore, combining with the result in 1, if A is injective on $\mathcal{A}^1(\Omega)$ and $A1 \neq 0$, Equation 16 is strictly convex, thus its minimizer has to be unique. \square

6 Algorithms

In this section we will introduce the algorithms needed for the following numerical simulations. First we will give the notations and discretization of the different operators that our algorithms will require. To keep the notations simple, we re-use the same symbols as in continuous case in the previous sections for the discrete case. Then, we will propose a method for estimating the main direction in images. In the end of the section, we will propose a primal-dual based algorithm for solving the minimization problem in the L^2 - DTGV_λ^2 model.

6.1 Notations and discretization

The domain Ω is discretized as an M -by- M equidistant pixel-grid with pixel-size 1×1 . We use (i, j) to denote a pixel indice with $1 \leq i, j \leq M$, such that $u_{i,j}$ gives the pixel value at (i, j) . Here, for the sake of simplicity we stick to a square pixel-grid, but all proposed algorithms can be easily generalized to any rectangular discretization.

For $u \in \mathbb{R}^{M \times M}$, the discrete gradient operator $\nabla : \mathbb{R}^{M \times M} \rightarrow \mathbb{R}^{2M \times M}$ is defined as

$$\nabla u = \begin{pmatrix} \nabla_{x_1}^+ u \\ \nabla_{x_2}^+ u \end{pmatrix},$$

where $\nabla_{x_1}^+$ and $\nabla_{x_2}^+$ are obtained by applying forward finite difference scheme with symmetric boundary condition, i.e.,

$$\begin{aligned} (\nabla_{x_1}^+ u)_{i,j} &= \begin{cases} u_{i+1,j} - u_{i,j}, & \text{if } i < M, \\ 0, & \text{if } i = M, \end{cases} \quad \text{and} \\ (\nabla_{x_2}^+ u)_{i,j} &= \begin{cases} u_{i,j+1} - u_{i,j}, & \text{if } j < M, \\ 0, & \text{if } j = M. \end{cases} \end{aligned}$$

The divergence operator is defined as the adjoint operator of ∇ , i.e., we have $\text{div} = -\nabla^* = (\nabla_{x_1}^-, \nabla_{x_2}^-)$, where $\nabla_{x_1}^-$ and $\nabla_{x_2}^-$ utilize the backward finite difference scheme. Moreover, based on Equation 9, the directional divergence can be obtained by calculating $\widetilde{\text{div}} = \text{div} R_\theta \Lambda_a$, and the corresponding directional gradient operator is $\widetilde{\nabla} = \Lambda_a R_{-\theta} \nabla$.

For a tensor W with $W_{i,j} = \begin{pmatrix} w_{i,j}^{11} & w_{i,j}^{12} \\ w_{i,j}^{12} & w_{i,j}^{22} \end{pmatrix}$ and $1 \leq i, j \leq M$, its divergence can be expressed as

$$(\text{div} W)_{i,j} = \begin{pmatrix} (\nabla_{x_1}^+ w^{11})_{i,j} + (\nabla_{x_2}^+ w^{12})_{i,j} \\ (\nabla_{x_1}^+ w^{12})_{i,j} + (\nabla_{x_2}^+ w^{22})_{i,j} \end{pmatrix}.$$

Based on the definition in Equation 9, the directional divergence, $\widetilde{\text{div}}$, can be obtained by calculating

$$(\widetilde{\text{div}} W)_{i,j} = (\text{div} \widetilde{W})_{i,j} \quad \text{with} \quad \widetilde{W}_{i,j} = R_\theta \Lambda_a W_{i,j}.$$

In addition, for a tensor \mathbf{v} with $\mathbf{v}_{i,j} = (v_{i,j}^1, v_{i,j}^2)^\top$ and $1 \leq i, j \leq M$, its directional symmetrized derivative is given by

$$(\widetilde{\mathcal{E}} \mathbf{v})_{i,j} = \frac{1}{2} \left[\Lambda_a R_\theta \begin{pmatrix} (\nabla_{x_1}^- v^1)_{i,j} & (\nabla_{x_1}^- v^2)_{i,j} \\ (\nabla_{x_2}^- v^1)_{i,j} & (\nabla_{x_2}^- v^2)_{i,j} \end{pmatrix} + \begin{pmatrix} (\nabla_{x_1}^- v^1)_{i,j} & (\nabla_{x_2}^- v^1)_{i,j} \\ (\nabla_{x_1}^- v^2)_{i,j} & (\nabla_{x_2}^- v^2)_{i,j} \end{pmatrix} R_\theta^\top \Lambda_a \right]$$

Note that for tensors it still holds that $\widetilde{\text{div}} = -\widetilde{\mathcal{E}}^*$.

6.2 Detecting main direction in images

In order to apply DTGV as regularization, the parameters a and θ have to be specified. In this paper, we focus on the case that the objects in images are mainly along only one direction. By estimating this main direction, we will obtain the parameter θ . The parameter a somehow shows the confidence on the angle estimation. For image restoration, the main direction can be estimated directly from the degraded images. Some classical methods to estimate angles or directions in images could used here, e.g., 2D Fourier transform and the arctangent function with two arguments. There are also more advanced techniques for angle estimation. Here we list a few of them: the quadrature filter [17], the boundary tensor [17], and the structure tensor [35]. Most of these methods estimate the direction pixel-wisely, but in our case we aim for only one main direction for the whole image. In this section, based on our single direction assumption, we will introduce another method to estimate the main direction and test on a series of noisy images.

Our direction estimator refers to the work in [29], and is mainly composed of three steps. First, we smooth the degraded image in order to reduce the influence

of noise. Then, a pixel-wise angle estimation is calculated as

$$\Theta_{i,j} = \begin{cases} 0, & \text{if } |(\nabla f^\sigma)_{i,j}|_2 < 10^{-3}, \\ \arccos\left(\frac{(\nabla_{x_1}^+ f^\sigma)_{i,j}}{|(\nabla f^\sigma)_{i,j}|_2}\right), & (\nabla_{x_2}^+ f^\sigma)_{i,j} \geq 0 \text{ and } |(\nabla f^\sigma)_{i,j}|_2 < 10^{-3}, \\ 2\pi - \arccos\left(\frac{(\nabla_{x_1}^+ f^\sigma)_{i,j}}{|(\nabla f^\sigma)_{i,j}|_2}\right), & \text{otherwise,} \end{cases} \quad (17)$$

where f^σ denotes the smoothed image from the first step. After that, we smooth the estimated angles in order to remove the outlier due to the noise and small features. At the same time, we introduce the new period for the angles. Note that in [29] the focus is on restoring rectangle shapes, therefore $\pi/2$ -period is used. But in our case, we need π -period for angles. Moreover, we only need the main direction in the image, which is obtained by calculating the mean. In 1 the details of the main direction estimation method are outlined. We should notice that if we do not calculate the mean of the angles, then we would have pixel-wise angle estimation, which would be utilized for restoring images with multiple angles in the future.

Algorithm 1 Main Direction Estimation Method

- 1: Input smoothing parameter μ and the degraded image f .
 - 2: Smooth the degraded image by implementing Gaussian blur: $f^\sigma = G_\sigma f$, where G_σ denotes Gaussian blurring operator with mean 0 and variance σ^2 .
 - 3: Estimate pixel-wise direction Θ^u according to Equation 17.
 - 4: Introduce $\frac{\pi}{2}$ -period to the angles and smooth them:
 - 5: $c_{i,j}^u = \cos(4\Theta_{i,j}^u)$,
 - 6: $s_{i,j}^u = \sin(4\Theta_{i,j}^u)$,
 - 7: $(c^v, s^v) =$
 - 8: $\arg \min_{c^v, s^v} \sum_{i,j} |(\nabla f)_{i,j}|_2^2 \left| \begin{pmatrix} c_{i,j}^u \\ s_{i,j}^u \end{pmatrix} - \begin{pmatrix} c_{i,j}^v \\ s_{i,j}^v \end{pmatrix} \right|_2^2 + \mu \left(|(\nabla c^v)_{i,j}|_2^2 + |(\nabla s^v)_{i,j}|_2^2 \right)$.
 - 9: The smoothed pixel-wise angles, Θ^v , are obtained by implementing Equation 17 with (c^v) instead of ∇f^σ as input.
 - 10: Calculate the main direction: $\theta = \frac{1}{|\Omega|} \sum_{i,j} \Theta_{i,j}^v$.
 - 11: Transform into π -periodic angle according to
 - 12: $\theta \leftarrow \begin{cases} -\theta, & \text{if } (\nabla_{x_1}^+ f^\sigma) : (\nabla_{x_2}^+ f^\sigma) \leq 0, \\ \frac{\pi}{2} - \theta, & \text{otherwise,} \end{cases}$
 - 13: where “:” denotes the Frobenius inner product, which is defined in the proof of 3.2.
 - 14: **return** θ .
-

6.3 The Chambolle-Pock algorithm

First, corresponding to Equation 16 we formulate the discrete L^2 -DTGV $_\lambda^2$ model as

$$\operatorname{argmin}_{u \in \mathbb{R}^{M \times M}} \mathcal{J}(u) := \frac{1}{2} \|Au - f\|_F^2 + \operatorname{DTGV}_\lambda^2(u). \quad (18)$$

Since the minimization problem in Equation 18 is convex, many optimization algorithms could be used to solve it, e.g. Nesterovs method [21], the FISTA algorithm [3], the alternating direction method with multipliers (ADMM) [4], and any of the many primal-dual-based methods. Here, due to the simplicity of the implementation, we utilize the Chambolle-Pock primal-dual (CP) algorithm [8] to solve our problem.

Referring to the algorithm proposed in [5], we can rewrite the data-fitting term in Equation 18, $\mathcal{F}(u) = \frac{1}{2}\|Au - f\|_F^2$, as

$$\mathcal{F}(u) = \max_{q \in \mathcal{U}} \langle Au, q \rangle - \frac{1}{2}\|q\|_2^2 - \langle f, q \rangle, \quad (19)$$

where $\mathcal{U} = \mathbb{R}^{M \times M}$. Combining with the result in 4.1, we obtain the primal-dual formulation of Equation 18

$$\min_{u \in \mathcal{U}, \mathbf{v} \in \mathcal{V}} \max_{q \in \mathcal{U}, \mathbf{p} \in \mathcal{P}, W \in \mathcal{W}} \langle Au, q \rangle - \frac{1}{2}\|q\|_2^2 - \langle f, q \rangle + \langle \tilde{\nabla}u - \mathbf{v}, \mathbf{p} \rangle + \langle \tilde{\mathcal{E}}\mathbf{v}, W \rangle$$

where $\mathcal{V} = \mathbb{R}^{2M \times M}$, $\mathcal{P} = \{\mathbf{p} : \Omega \rightarrow \mathbb{R}^2 \mid \|\mathbf{p}_{i,j}\|_2 \leq \lambda_1 \text{ for } \forall(i,j) \in \Omega\}$, $\mathcal{W} = \{W : \Omega \rightarrow \text{Sym}^2(\mathbb{R}^2) \mid \|W_{i,j}\|_F \leq \lambda_0 \text{ for } \forall(i,j) \in \Omega\}$. This is a generic saddle-point problem, and we can apply the CP algorithm proposed in [8] to solve it. The algorithm is summarized in Algorithm 2.

In Algorithm 2, η and τ denote the dual and primal step-sizes, respectively. In addition, \mathcal{S}_λ is a set-projection operator defined as

$$[\mathcal{S}_\lambda(\xi)]_{i,j} = \frac{\xi_{i,j}}{\max\left(1, \frac{|\xi_{i,j}|}{\lambda}\right)}.$$

If $\xi \in \mathcal{P}$, then $|\xi_{i,j}|$ is with 2-norm; and if $\xi \in \mathcal{W}$, then $|\xi_{i,j}|$ is with Frobenius norm. Here, we use the relative changes of the objective function in Equation 18 to define the stopping criterion, since the objective function is essentially what we desire to minimize and its calculation can be simply implemented.

7 Numerical Experiments

In this section, we provide numerical results to study the behavior of our method. First, we examine the direction estimation method proposed in 1 for a series of noisy images, ranging from low- to high-level noise. Since the directional regularization requires additional parameters (θ, a) , we then empirically examine how these parameters influence the solution of Equation 18. In the end, we compare DTGV $^2_\lambda$ - and DTV-regularization with TGV $^2_\lambda$ - and classical TV-regularization for some denoising and deblurring problems, where the blurring and noise have been simulated. Based on the balance between the computational complexity and the result improvement, the second order of TGV is mostly widely used, so in our numerical experiments we only investigate DTGV $^2_\lambda$ and compare it with TGV $^2_\lambda$. To simplify the notations, we refer to TGV $^2_\lambda$ and DTGV $^2_\lambda$ as TGV and DTGV in this section. In addition, same as in [6] we fix the ratio between the two regularization parameters, i.e., $\frac{\lambda_0}{\lambda_1} = 2$, which commonly yields good restoration results. The tolerance in the 2 has been chosen as 10^{-6} and all simulated experiments are implemented in Matlab.

Algorithm 2 The CP algorithm for solving L^2 -DTGV $_{\lambda}^2$

- 1: Require f, A, λ, a, θ and tol.
- 2: Estimate Lipschitz constant L , e.g. using power-method for A .
- 3: Initialize $u^0 = \bar{u}^0 = 0, v^0 = 0, q^0 = 0, p^0 = \bar{p}^0 = 0, w^0 = 0, e^0 = 0, \eta < \frac{1}{\sqrt{L}}, \tau < \frac{1}{\sqrt{L}}$.
- 4: Run loop until stopping criterion is met:
- 5: **while** $e^k > \text{tol}$ **do**

$$\begin{aligned}
\mathbf{p}^{k+1} &= \arg \max_{\mathbf{p} \in \mathcal{P}} \langle \tilde{\nabla} \bar{u}^k - \bar{\mathbf{v}}^k, \mathbf{p} \rangle - \frac{1}{2\eta} \|\mathbf{p} - \mathbf{p}^k\|_2^2 \\
&= \mathcal{S}_{\lambda_1} \left(\mathbf{p}^k + \eta \left(\tilde{\nabla} \bar{u}^k - \bar{\mathbf{v}}^k \right) \right) \\
W^{k+1} &= \arg \max_{W \in \mathcal{W}} \langle \tilde{\mathcal{E}} \bar{\mathbf{v}}^k, W \rangle - \frac{1}{2\eta} \|W - W^k\|_F^2 \\
&= \mathcal{S}_{\lambda_0} \left(W^k + \eta \tilde{\mathcal{E}} \bar{\mathbf{v}}^k \right) \\
q^{k+1} &= \arg \max_{q \in \mathcal{U}} \langle A \bar{u}^k, q \rangle - \frac{1}{2} \|q\|_2^2 - \langle f, q \rangle - \frac{1}{2\eta} \|q - q^k\|_2^2 \\
&= \frac{1}{1 + \eta} \left(q^k + \eta (A \bar{u}^k - f) \right) \\
u^{k+1} &= \arg \min_{u \in \mathcal{U}} \langle Au, q^{k+1} \rangle + \langle \tilde{\nabla} u, \mathbf{p}^{k+1} \rangle + \frac{1}{2\tau} \|u - u^k\|_2^2 \\
&= u^k + \tau \left(\tilde{\text{div}} \mathbf{p}^{k+1} - A^* q^{k+1} \right) \\
\mathbf{v}^{k+1} &= \arg \min_{\mathbf{v} \in \mathcal{V}} -\langle \mathbf{v}, \mathbf{p}^{k+1} \rangle + \langle \tilde{\mathcal{E}} \mathbf{v}, W^{k+1} \rangle + \frac{1}{2\tau} \|\mathbf{v} - \mathbf{v}^k\|_2^2 \\
&= \mathbf{v}^k + \tau \left(\mathbf{p}^{k+1} + \tilde{\text{div}} W^{k+1} \right) \\
\bar{u}^{k+1} &= 2u^{k+1} - u^k \\
\bar{\mathbf{v}}^{k+1} &= 2\mathbf{v}^{k+1} - \mathbf{v}^k \\
e^{k+1} &= \frac{|\mathcal{J}(u^k) - \mathcal{J}(u^{k+1})|}{\mathcal{J}(u^k)}
\end{aligned}$$

end while

- 6: **return** u^{k+1} .
-

7.1 Robustness of direction-estimation

Since the estimation of the main direction plays an important role in our method, we first demonstrate the performance of the presented direction-estimation method in 1. Here, we use one simulated image and one real image for numerical experiments, and test our direction-estimation method on the images with up to 50% Gaussian noise. In all tests, we set $\sigma = 10$ for the smoothing step, i.e., Step 2 in 1. The numerical results are shown in Figure 3. It is clear that for both test images until the noise level (nl) reaching to 20% our method provides good estimation to the main direction. Especially for the real image, even with 50% noise, the estimation is still very accurate.

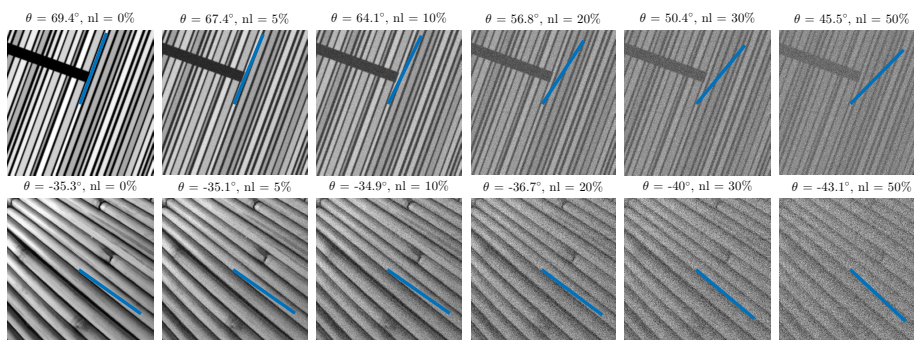


Figure 3: Estimating main direction in test images with increasing noise-level (nl). The top image size is 512×512 and bottom one is 253×253 . Main direction estimate θ is written in degrees and visualized on top of the noisy images with a blue line from the center.

7.2 Role of DTGV parameters

In the DTGV functional, except the parameter λ there are another two important parameters: θ and a , where θ shows the main direction and a demonstrates to what extent the textures in images following this main direction. If $a = 1$, the DTGV becomes identical to the rotation invariant TGV. In this section, we will test the influence of these two parameters when DTGV is used as a regularizer, and also seek the robustness of the L^2 - DTGV solutions with respect to their selections.

In order to study the influence from a and θ solely, in each test with fixed values for (a, θ) we adjust the regularization parameter λ and pick the one that provides the highest peak signal-to-noise ratio (PSNR) value. In Figure 4-7, we use two simulated images and two real images. Since the test image in Figure 4 is piece-wise constant, the DTV is used as regularizer instead. All test images are corrupted by 5% Gaussian noise, and the blurring operator A is set as identity. In Figure 4-7, we visualize the PSNR values for different choice of (a, θ) , where we test $a \in [0.01, 0.45]$ and $\theta \in [\bar{\theta} - 20^\circ, \bar{\theta} + 20^\circ]$ with $\bar{\theta}$ as the estimated main direction by 1. In addition, for each test image we also show three restoration results: the best one, the one with wrong θ and small a , and the one with correct θ and large a .

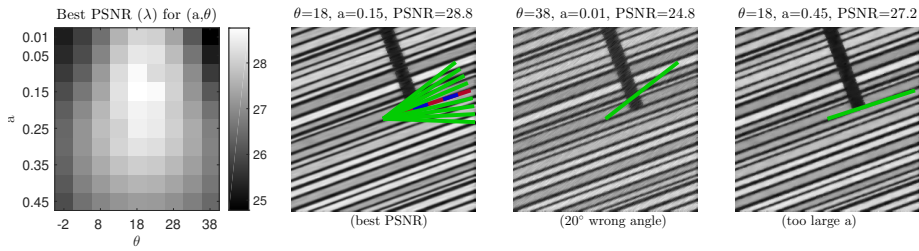


Figure 4: Test image 1: piece-wise constant image. DTV-regularized denoising problem. Lines mark specific angles: **tested angles**, **estimated angle** and **best angle**.

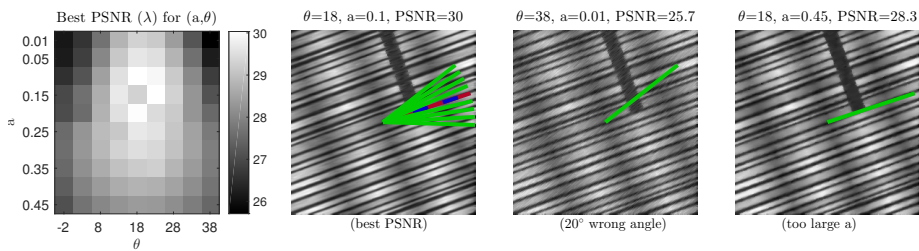


Figure 5: Test image 2: piece-wise affine image. DTGV-regularized denoising problem. Lines mark specific angles: **tested angles**, **estimated angle** and **best angle**.

Obviously, the use of directional regularization improves the PSNR values significantly when θ coincides with the main direction of the image. Moreover, with a good direction estimation the highest PSNR values are usually achieved by choosing a relatively small a . In addition, from the restored images we can see that with incorrect θ and a small a there are some line artifacts along the direction of θ . The reason is that with a small a the textures in the images are forced to be restored along the incorrect direction. With correct θ and a large a the restored results look very close to the TV- or TGV-regularized results. Especially in the last figure of Figure 4, staicasing artifact starts to appear.

The tests in Figure 4-7 also can serve as robustness tests for our method. They show that our method is robust with respect to the parameters for $a \in [0.1, 0.2]$ and θ within $[\bar{\theta} - 5^\circ, \bar{\theta} + 5^\circ]$. So in the following numerical experiments, we will use 1 to estimate θ and fix a to 0.15.

7.3 Image denoising

To show the improvement of imposing the direction prior into the regularization we empirically compare DTGV and DTV with TGV and TV for the image denoising problem. We use four different test-images with 10% and 20% Gaussian noise respectively. In all tests, after many experiments with different choices of the regularization parameter λ , the ones that provide the best PSNRs are presented here.

Comparing the results from the four different regularization techniques in Figure 8 and Figure 9, we see that both visually and quantitatively in terms of PSNR

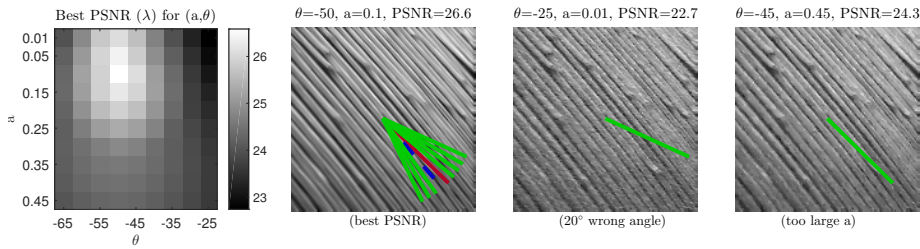


Figure 6: Test image 3: real image. DTGV-regularized denoising problem. Lines mark specific angles: **tested angles**, **estimated angle** and **best angle**.

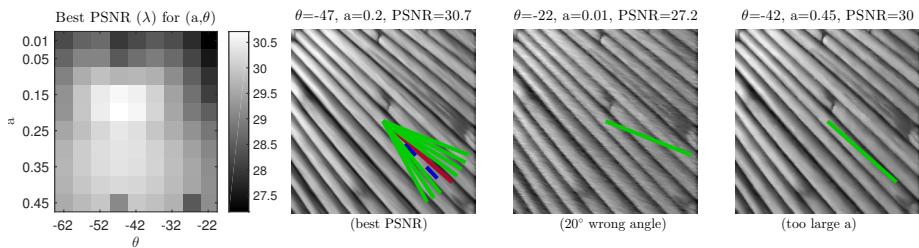


Figure 7: Test image 4: real image. DTGV-regularized denoising problem. Lines mark specific angles: **tested angles**, **estimated angle** and **best angle**.

the improvement by directional regularizers is evident. Especially the PSNR values from the results by solving L^2 -DTGV model are more than 2.2dB higher than the ones from L^2 -TGV model. The textures in the images are obviously much better preserved by using DTV and DTGV than by using the two isotropic methods, i.e., TV and TGV. Note that in both results from TV and DTV for the second test image, the stair-casing artifact is observable along the main direction. This is due to the test image being piecewise affine, while the TV and DTV regularizers are based on an assumption of piece-wise constant. In this case, by using DTGV as regularization the artifacts are successfully removed and the textures are well preserved. Hence, these tests demonstrate the advantages of including directional information in the regularizer when dealing with directional images.

In the first two simulated test images, we specially add a dark region perpendicular to the main direction in order to demonstrate the potential artifacts from the directional regularizers. We can see that near the boundary of the dark region there appear some artifacts in the restored results by DTV and DTGV. It is due to the diffusion of the different intensities along the main direction. In addition, the similar artifacts can be observed in the results from DTV and DTGV for restoring the two real images, especially at the textures that are almost perpendicular to the main direction. In order to clearly show these artifacts, in [Figure 10](#) we zoomed in a corner of the last test image and show the comparison of the four restorations. These artifacts mainly occur when the direction prior is not met, e.g. a part of textures in the images do not follow the main direction.

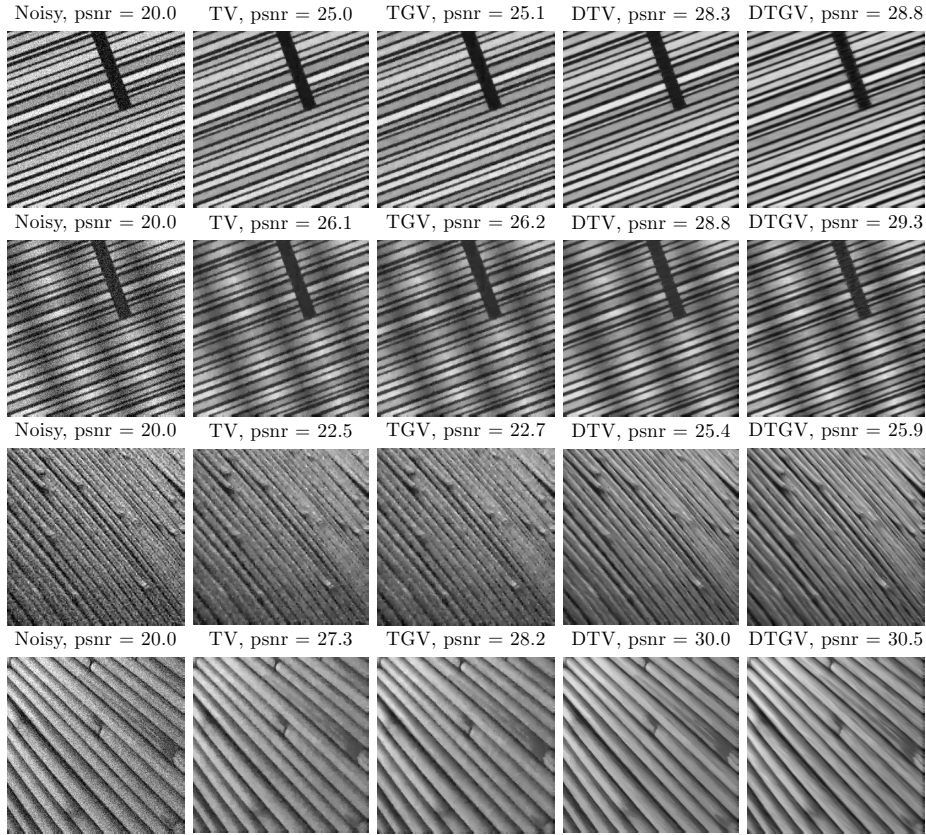


Figure 8: Comparison of TV, TGV, DTV and DTGV regularizations for four different denoising problems with 10% Gaussian noise.

7.4 Image deblurring and denoising

In order to test directional regularization on a more complicated problem, we consider the restoration of the noisy blurred images. In our experiment, the blurring operator is set as Gaussian blur with a window size 7×7 and a standard deviation of 2. Further, after blurred, the test image is corrupted by 10% Gaussian noise. In our method, we still use 1 to estimate the main direction in the image.

In Figure 11, we show the degraded image and the restored results by using TV, TGV, DTV and DTGV regularizations. It is clear that both TV and TGV cannot help to restore the edges correctly, while the directional methods are much better on restoring the textures and removing the noise. In addition, the DTV solution is seen be heavily influenced by the stair-casing artifacts, since this test image is piece-wise affine and is not fit with the piece-wise constant assumption for TV-based method. Due to the use of higher order derivatives, those artifacts do not appear in the DTGV solution, as expected. Quantitatively, the PSNR value is increased by at least 2.6dB when the directional regularizer is utilized.

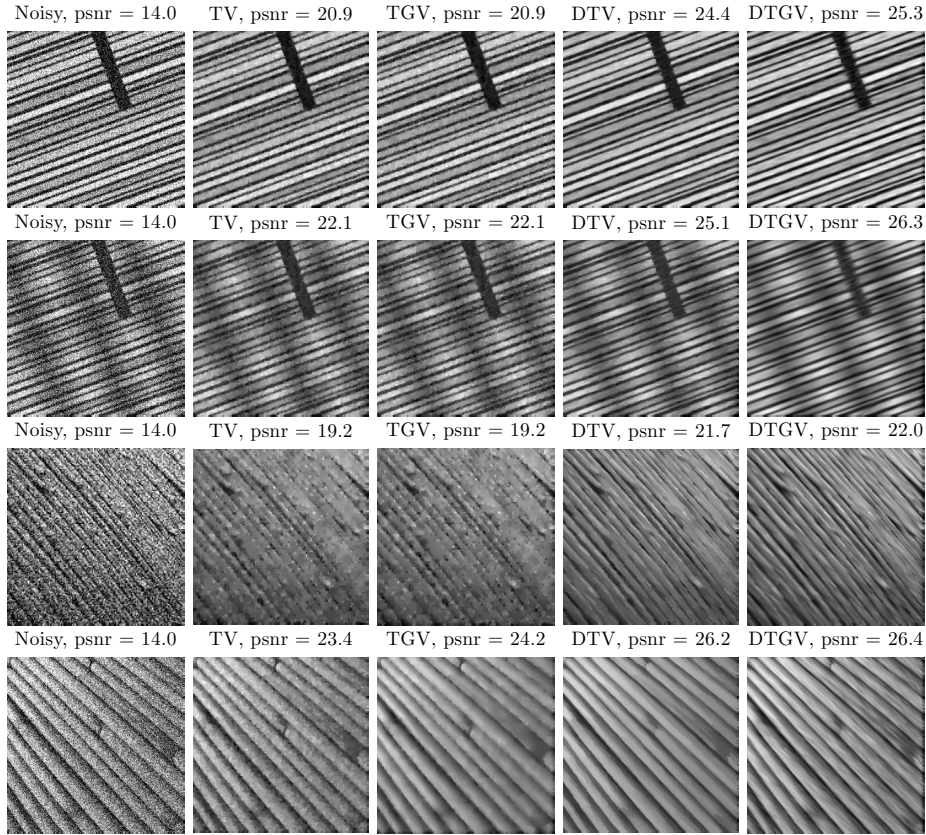


Figure 9: Comparison of TV, TGV, DTV and DTGV regularizations for four different denoising problems with 20% Gaussian noise.

8 Conclusion

In this paper, we propose a new directional functional, directional total generalized variation (DTGV), and study its mathematical properties. Then we combine DTGV with the least-squares data-fitting term and propose a new variational model, L^2 -DTGV, for restoring images whose texture mainly follow one direction. We prove the existence and the uniqueness of a solution to our proposed model, and apply the primal-dual algorithm to solve the corresponding minimization problem in the new model. Since the new proposed DTGV functional requires the input of the main direction for the images, we also propose a direction estimation algorithm, which can be easily extended to spatially varying direction estimation. Numerical results show that the direction estimation algorithm is reliable and the improvement for restoring directional images by using DTGV as regularizer is significant comparing with isotropic regularizers. In addition, we also try to discover the potential artifacts from DTGV. In order to reduce the artifacts from DTGV, we intend to extend our method to deal with multi-directions in the future.

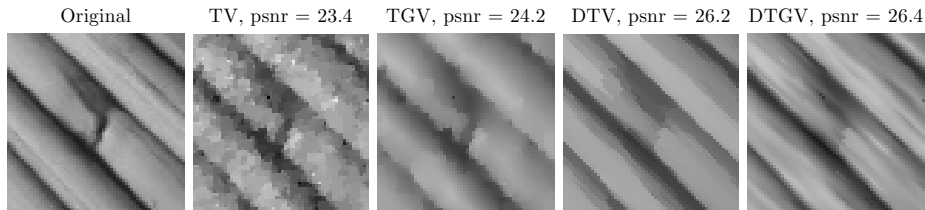


Figure 10: The zoomed-in regions of the restored results shown in the last row of Figure 9.

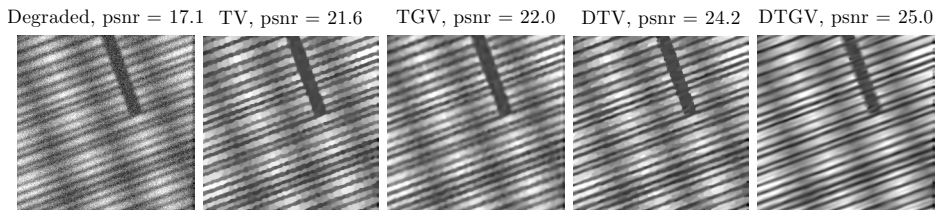


Figure 11: Comparison of TV, TGV, DTV and DTGV regularizations for a piecewise affine noisy blurred image.

Acknowledgements

The work was supported by Advanced Grant 291405 from the European Research Council and grant no. 4002-00123 from the Danish Council for Independent Research Natural Sciences.

References

- [1] G. Aubert and P. Kornprobst. *Mathematical problems in image processing: partial differential equations and the calculus of variations*. 2006.
- [2] I. Bayram and M. E. Kamasak. A directional total variation. *Eur. Signal Process. Conf.*, 19(12):265–269, 2012.
- [3] A. Beck and M. Teboulle. A Fast Iterative Shrinkage-Thresholding Algorithm for Linear Inverse Problems. *SIAM J. Imaging Sci.*, 2(1):183–202, jan 2009.
- [4] S. Boyd, N. Parikh, E. Chu, B. Peleato, and J. Eckstein. Distributed Optimization and Statistical Learning via the Alternating Direction Method of Multipliers. *Found. Trends[®] Mach. Learn.*, 3(1):1–122, 2010.
- [5] K. Bredies. Recovering piecewise smooth multichannel images by minimization of convex functionals with total generalized variation penalty. *Lect. Notes Comput. Sci. (including Subser. Lect. Notes Artif. Intell. Lect. Notes Bioinformatics)*, 8293:44–77, 2014.
- [6] K. Bredies, K. Kunisch, and T. Pock. Total Generalized Variation. *SIAM J. Imaging Sci.*, 3(3):492–526, 2010.

- [7] K. Bredies and T. Valkonen. Inverse problems with second-order total generalized variation constraints. *Int. Conf. Sampl. Theory Appl.*, pages 1–4, 2011.
- [8] A. Chambolle and T. Pock. A first-order primal-dual algorithm for convex problems with applications to imaging. *J. Math. Imaging Vis.*, 40(1):120–145, dec 2011.
- [9] T. Chan, A. Marquina, and P. Mulet. High-Order Total Variation-Based Image Restoration. *SIAM J. Sci. Comput.*, 22(2):503–516, 2000.
- [10] T. F. Chan and C. K. Wong. Total variation blind deconvolution. *IEEE Trans. Image Process.*, 7(3):370–5, 1998.
- [11] A. H. Delaney and Y. Bresler. Globally convergent edge-preserving regularized reconstruction: An application to limited-angle tomography. *IEEE Trans. Image Process.*, 7(2):204–221, 1998.
- [12] Y. Dong, M. Hintermüller, and M. Neri. An efficient primal-dual method for L^1 TV image restoration. *SIAM Journal on Imaging Sciences*, 2(4):1168–1189, 2009.
- [13] Y. Dong and T. Zeng. A convex variational model for restoring blurred images with multiplicative noise. *SIAM Journal on Imaging Sciences*, 6(3):1598–1625, 2013.
- [14] G. R. Easley, D. Labate, and F. Colonna. Shearlet-based total variation diffusion for denoising. *IEEE Trans. Image Process.*, 18(2):260–268, 2009.
- [15] V. Estellers, S. Soatto, and X. Bresson. Adaptive Regularization With the Structure Tensor. *IEEE Trans. Image Process.*, 24(6):1777–1790, 2015.
- [16] X. Fei, Z. Wei, and L. Xiao. Iterative Directional Total Variation Refinement for Compressive Sensing Image Reconstruction. *Signal Process. Lett. IEEE*, 20(11):1070–1073, 2013.
- [17] G. H. Granlund and H. Knutsson. *Signal Processing for Computer Vision*. Springer-Science+Business Media Dordrecht, 1995.
- [18] K. M. Jespersen, J. Zangenberg, T. Lowe, P. J. Withers, and L. P. Mikkelsen. Fatigue damage assessment of uni-directional non-crimp fabric reinforced polyester composite using X-ray computed tomography. *Submitted*, 136:94–103, 2015.
- [19] E. Jonsson, T. Chan, and S.-C. Huang. Total Variation Regularization in Positron Emission Tomography. Technical report, Dept. Mathematics, Univ. California., Los Angeles., 1998.
- [20] S. Lefkimmiatis, A. Roussos, P. Maragos, and M. Unser. Structure Tensor Total Variation. *SIAM J. Imaging Sci.*, 8(2):1090–1122, 2015.
- [21] Y. Nesterov. A method of solving a convex programming problem with convergence rate $O(1/k^2)$. *Sov. Math. Dokl.*, 27(2):372–376, 1983.
- [22] M. Nikolova. Local Strong Homogeneity of a Regularized Estimator. *SIAM J. Appl. Math.*, 61(2):633–658, 2000.

- [23] W. Ring. Structural properties of solutions to total variation regularization problems. *ESAIM Math. Model. Numer. Anal. - Modélisation Mathématique Anal. Numérique*, 34(4):799–810, 2000.
- [24] L. I. Rudin, S. Osher, and E. Fatemi. Nonlinear total variation based noise removal algorithms. *Phys. D Nonlinear Phenom.*, 60(1-4):259–268, 1992.
- [25] S. R. Sandoghchi, G. T. Jasion, N. V. Wheeler, S. Jain, Z. Lian, J. P. Wooler, R. P. Boardman, N. K. Baddela, Y. Chen, J. R. Hayes, E. N. Fokoua, T. Bradley, D. R. Gray, S. M. Mousavi, M. N. Petrovich, F. Poletti, and D. J. Richardson. X-ray tomography for structural analysis of microstructured and multimaterial optical fibers and preforms. *Opt. Express*, 22(21):26181, 2014.
- [26] O. Scherzer. Denoising with higher order derivatives of bounded variation and an application to parameter estimation. *Computing*, 60(1):1–27, 1998.
- [27] F. Sciacchitano, Y. Dong, and T. Zeng. Variational approach for restoring blurred images with Cauchy noise. *SIAM Journal on Imaging Sciences*, 8(3):1894–1922, 2015.
- [28] S. Setzer and G. Steidl. Variational methods with higher order derivatives in image processing. *Approx. Theory XII San Antonio 2007*, pages 360–385, 2008.
- [29] S. Setzer, G. Steidl, and T. Teuber. Restoration of images with rotated shapes. *Numer. Algorithms*, 48(1-3):49–66, 2008.
- [30] S. Setzer, G. Steidl, and T. Teuber. Infimal convolution regularizations with discrete l_1 -type functionals. *Commun. Math. Sci.*, 9(3):797–827, 2011.
- [31] R. Temam. *Mathematical Problems in Plasticity*. Gauthier-Villars, 1985.
- [32] E. Turgay and G. B. Akar. Directionally adaptive super-resolution. *2009 16th IEEE Int. Conf. Image Process.*, (1):1201–1204, 2009.
- [33] C. R. Vogel and M. E. Oman. Iterative Methods for Total Variation Denoising. *SIAM J. Sci. Comput.*, 17(1):227–238, 1996.
- [34] J. Weickert. Coherence-Enhancing Diffusion Filtering. *Int. J. Comput. Vis.*, 31(2):111–127, 1999.
- [35] J. Weickert, B. Romeny, and M. Viergever. Efficient and reliable scheme for nonlinear diffusion filtering. *T-IP*, 7(3):398–410, 1998.
- [36] H. Zhang and Y. Wang. Edge adaptive directional total variation. *J. Eng.*, (October):1–2, 2013.